Sensitivity analysis of neutron total and absorption cross sections within the optical model

M. T. Pigni,* M. Herman, and P. Obložinský
National Nuclear Data Center, Brookhaven National Laboratory, Upton, New York 11973-5000, USA

F. S. Dietrich
National Nuclear Data Center, Brookhaven National Laboratory, Upton, New York 11973-5000, USA and
Mail Stop L-414, Lawrence Livermore National Laboratory, Livermore, California 94551, USA
(Received 20 August 2010; published 2 February 2011)

Distinct maxima and minima in neutron total and absorption cross-section uncertainties when optical-model parameters are varied have been observed in large-scale covariance calculations. These features were seen over a wide mass range (20–210) and for energies up to 20 MeV. Here we investigate the physical origin of the observed patterns over an extended energy range (1 keV to 200 MeV). We have calculated the sensitivity of the cross sections for a specific nucleus (^{56}Fe) to variations of the 15 parameters of a standard global optical potential parametrization, and have also carried out calculations for alternative global optical potentials over the original wide mass and energy ranges. We find that simple physical descriptions can be found in two energy ranges. Below approximately 100 keV, the patterns arise from the interplay of the *s*- and *p*-wave single-particle resonances. Above approximately 4 MeV, a single-phase-shift approximation (the Ramsauer model) describes the observed behavior. We discuss the potential importance of such sensitivity studies for further development of optical potentials.

DOI: 10.1103/PhysRevC.83.024601 PACS number(s): 24.10.Ht, 25.40.−h, 28.20.Cz, 28.20.Fc

I. INTRODUCTION

In recent years there has been renewed interest in quantitative assessment of uncertainties in neutron-induced cross sections, driven largely by the requirements of advanced concepts for nuclear power reactors and other applications. The subject is of broader interest as it requires a detailed assessment of nuclear reaction theory and its parameters, which are taken from basic nuclear physics studies, including their uncertainties and correlations. Such nuclear reaction calculations are very important for evaluating existing experimental data and are essential where no data are available. These calculations, mainly based on the Hauser-Feshbach formalism [1], are suitable for describing experimental data when such data are averaged over an appropriate energy interval. A current assessment of the relevant models and parameters can be found in Ref. [2].

The optical model is a critically important ingredient in such nuclear reaction calculations, because it yields the cross section for compound nuclear formation in the initial stage of a reaction and supplies the transmission coefficients for branching into the various final states. Because of its importance, a large-scale covariance study was recently carried out [3] to assess the sensitivity of a wide variety of neutron-induced reactions to variations in the parameters describing the optical model. This study was carried out for nuclei across the periodic table (^{19}F to ^{209}Bi) and for a broad range of neutron energies (up to 20 MeV). For the present work, the study was extended up to 200 MeV. At the upper energies, the optical model has additional importance in determining the properties of the direct and preequilibrium reactions that precede the formation of an equilibrated compound nucleus whose decays can be calculated using the Hauser-Feshbach or simpler evaporation mechanisms. When plotted on a mass-energy grid, these results show patterns of bands in which the total and absorption cross sections are very *insensitive* to certain optical-model parameters. The purpose of this article is to exhibit these features and to identify the physical ingredients that are responsible for them. Although we use a particular recent global optical-model parametrization for most of these investigations (that of Koning and Delaroche [4]), we show that alternative global parametrizations exhibit very similar patterns.

To illustrate the patterns of sensitivity we are investigating, we show in Fig. 1 results from Ref. [3], extended up to 200 MeV, for the sensitivity of the total cross section to variations of the parameters of the optical potential of Ref. [4]. The fractional uncertainty in the total cross section corresponding to a physically reasonable uncertainty in each optical model parameter was calculated, and the results were added in quadrature (see Ref. [3] for details). In this case, the most important parameters are the strength and radius of the real central potential; the relative importance of the various parameters is discussed below. The scale on the right of the figure shows that the dark bands correspond to regions that are very insensitive to the optical-model parameters, while the very light regions are highly sensitive to them.

We note that at low energies the regions of low sensitivity are associated with specific mass regions, whereas at high energies the dark bands become nearly horizontal and therefore are associated with specific energies rather than specific masses. We show that both low- and high-energy behavior can be understood via simple models. At very low energies, the cross sections are dominated by a single partial wave (the *s* wave), which leads to an interpretation in terms of the same

*pigni@bnl.gov

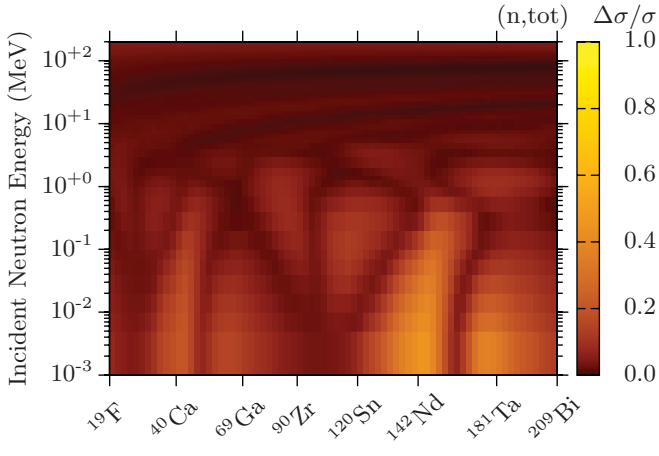

FIG. 1. (Color online) Relative uncertainties $\Delta\sigma/\sigma$ for neutron total neutron cross sections showing the patterns obtained by propagating uncertainties in the parameters of the Koning-Delaroche spherical optical potential [4].

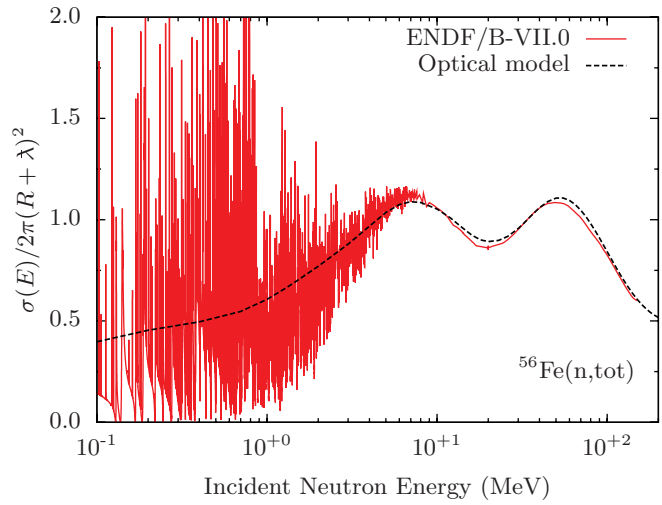

FIG. 2. (Color online) The total neutron cross section of ^{56}Fe. An optical-model calculation using the global potential of Ref. [4] is compared to the ENDF/B-VII.0 evaluation [7]. For clarity the cross section is divided by the black nucleus cross section, where $\lambda\!\!\!^{-}$ is the reduced wavelength and the radius R is $1.415A^{1/3}$ fm.

single-particle s-wave shell model states that give rise to the peaks in the s-wave neutron strength functions as a function of mass [5]. At somewhat larger energies, up to ≈100 keV, p waves are required to complete the picture. At high energies (≈4–100 MeV) the regularities can be explained by a different single-phase-shift model, the Ramsauer model [6], that corresponds to the interference between waves passing through the nucleus and those going around it. In between these two energy regions, a simple interpretation is not possible because the observed behavior results from the interplay of several partial waves.

The article is organized as follows. In Sec. II we provide a brief description of the optical model and the parametrization we are using, together with a description of the relevant observables. We also show explicit expressions for the sensitivity of the total and absorption cross sections in terms of the optical potential and the scattering wave function calculated from it. Section III contains the results of a sensitivity analysis for ^{56}Fe, which shows the sensitivities of the total and absorption cross sections to the individual optical-model parameters. The origin of the sensitivity minima and their stability to alternate choices of the optical potential parametrization are discussed in Sec. IV. Our findings are summarized in Sec. V.

II. OPTICAL MODEL AND OBSERVABLES

To illustrate what the present study is intended to address, we show in Fig. 2 an optical-model calculation for the total neutron cross section of ^{56}Fe, compared with a representation of the actual cross section taken from the ENDF/B-VII.0 evaluated nuclear data file [7]. At the lowest energies we see individual resonances. As the energy increases the resonances become dense and overlapping, yielding a cross section that fluctuates about an average value. At sufficiently high energies, these fluctuations damp out and yield a smooth energy dependence; this happens at about 5 MeV in the case shown. The optical model is designed to provide the *average* cross section over an energy interval large enough to contain many resonances. The sensitivity study examines the effect on the cross sections of varying the optical-model parameters and thus provides a measure of uncertainty in the average cross sections when they are calculated from an optical model.

The optical potential contains real and imaginary terms,

$$U(r, E) = V(r, E) + i\, W(r, E)\,, \tag{1}$$

each of which contains central and spin-orbit parts. The geometrical and strength dependencies are specified by a set of parameters, which we designate by $\{p_i\}$. This parametrization is not unique. We choose a common one that suffices for the phenomenological global potentials used in this work:

$$V = -V_v f(r, R_v, a_v) + V_{\rm so}\, \lambda\!\!\!^{-2}_{\pi}\, \frac{1}{r}\frac{d}{dr} f(r, R_{\rm vso}, a_{\rm vso})\mathbf{l}\cdot\boldsymbol{\sigma}\,, \tag{2}$$

$$W = -W_v f(r, R_w, a_w) + 4\, a_s\, W_s \frac{d}{dr} f(r, R_s, a_s) + W_{\rm so}\, \lambda\!\!\!^{-2}_{\pi}\, \frac{1}{r}\frac{d}{dr} f(r, R_{\rm wso}, a_{\rm wso})\mathbf{l}\cdot\boldsymbol{\sigma}\,, \tag{3}$$

where the radial form factor f is the Woods-Saxon shape

$$f(r, R_i, a_i) = \{1 + \exp[(r - R_i)/a_i]\}^{-1}\,, \tag{4}$$

and $\lambda\!\!\!^{-2}_{\pi}$ is the square of the reduced pion Compton wavelength, equal to 2.0 fm^2. We represent the radii as $R_i = r_i A^{1/3}$, where A is the target mass number.

The parameter set $\{p_i\}$ considered in the present work consists of the strength, reduced radius, and diffuseness parameters for the various components of the potential. The most important are $\{V_v, r_v, a_v\}$ for the real central potential, as well as $\{W_s, r_s, a_s\}$ and $\{W_v, r_w, a_w\}$ for the surface and volume imaginary central potentials, respectively. Also included, but of lesser importance, are $\{V_{\rm so}, r_{\rm vso}, a_{\rm vso}\}$ and $\{W_{\rm so}, r_{\rm wso}, a_{\rm wso}\}$ for the real and imaginary spin-orbit potentials, respectively. In

specific optical model implementations, the quantities $\{p_i\}$ are functions of additional parameters that characterize the energy dependence of the potential, as well as dependencies on other quantities such as target mass and isospin.

We have used the Koning-Delaroche global neutron potential [4] for most of the calculations. This is a recent spherical optical potential that has been determined by fitting a wide variety of experimental data from very low energies (the s- and p-wave strength functions) up to 200 MeV and over a wide mass region ($A = 24$ to 209). It is not intended for use with highly deformed nuclei, such as in the rare-earth region, since it is well established that these require a coupled-channels treatment. In the present work we have included the rare-earth region for the purpose of studying the systematics of a spherical potential, but it is understood that the results obtained in this region should not be compared with experiment.

The main neutron optical-model observables that we need in this article are the total and absorption cross sections. These may be expressed in terms of the S-matrix elements as

$$\sigma_{\rm tot} = 2\pi\lambda\!\!\!^{-2} \sum_{lj} \frac{1}{2}(2j+1)(1 - {\rm Re}\, S_{lj})\,, \tag{5}$$

$$\sigma_{\rm abs} = \pi\lambda\!\!\!^{-2} \sum_{lj} \frac{1}{2}(2j+1)(1 - |S_{lj}|^2). \tag{6}$$

In these expressions $\lambda\!\!\!^{-}$ is the reduced wavelength of the neutron, and the sum runs over all permitted values of l and j, where $j = l \pm \frac{1}{2}$. The S-matrix elements may be parametrized via the complex phase shifts δ_{lj} as $S_{lj} = \exp(2i\delta_{lj})$.

We now derive expressions that can be used to relate the optical-parameter sensitivities of the total and absorption cross sections directly to the optical potential itself and to the corresponding scattering wave functions. These will be particularly useful in discussing the cross-section sensitivities at low energies. We employ the partial-wave form of the well-known two-potential formula (see, for example, the discussion in Ref. [8]). Suppose that the scattering potential can be separated into two terms U and ΔU, so that the complete potential is $U + \Delta U$. The two-potential formula states that the S-matrix element for scattering from the complete potential, $S_{lj}(U + \Delta U)$, is related to that from the first term alone, $S_{lj}(U)$, by the expression

$$S_{lj}(U + \Delta U) = S_{lj}(U) + 2\pi I_{lj}\,, \tag{7}$$

where the integral I_{lj} is given by

$$I_{lj} = -\frac{2\mu}{\hbar^2}\,\frac{1}{k}\int_0^\infty dr\; \phi_{lj}^{(+)}(r)\;\Delta U(r)\;\chi_{lj}^{(+)}(r)\,, \tag{8}$$

in which μ is the reduced mass, k is the c.m. wave number, and $\phi_{lj}^{(+)}$ is a solution of the radial Schrödinger equation containing only the first part of the potential, U. The solution is chosen to have outgoing scattered-wave boundary conditions and the asymptotic normalization

$$\phi_{lj}^{(+)}(r) \underset{r\,\longrightarrow\,\infty}{\longrightarrow} e^{i\delta_{lj}}\sin(kr - l\frac{\pi}{2} + \delta_{lj})\,. \tag{9}$$

The function $\chi_{lj}^{(+)}$ has exactly the same form, except that the phase shift is replaced by one corresponding to the solution using the full potential $U + \Delta U$.

In the present case, we assume that an optical-model parameter p_i is altered by an infinitesimal amount δp_i, so that the new potential is $U + (\partial U/\partial p_i)\delta p_i$. We insert the second term of this expression in Eq. (8) for I_{lj}, and because the perturbation of the potential is very small, we replace $\chi_{lj}^{(+)}$ by $\phi_{lj}^{(+)}$. We compute the new S-matrix elements via Eq. (7) and insert these in the expressions for the cross sections, Eqs. (5) and (6). This yields the following expressions for the partial derivatives of the total and absorption cross sections with respect to the varied parameter:

$$\frac{\partial\sigma_{\rm tot}}{\partial p_i} = -\frac{2\mu}{\hbar^2}\,\frac{4\pi}{k^3}\sum_{lj}\frac{2j+1}{2}\,{\rm Im}\int_0^\infty dr\;\frac{\partial U}{\partial p_i}[\phi_{lj}^{(+)}]^2 \tag{10}$$

and

$$\frac{\partial\sigma_{\rm abs}}{\partial p_i} = -\frac{2\mu}{\hbar^2}\,\frac{4\pi}{k^3}\sum_{lj}\frac{2j+1}{2}\,{\rm Im}\int_0^\infty dr\;S_{lj}^*\frac{\partial U}{\partial p_i}[\phi_{lj}^{(+)}]^2. \tag{11}$$

In the low-energy limit, these expressions are identical because $S_{lj} \to 1$ in that limit. We also note that the cross-section derivatives for the real potential parameters can be expected to have very different behavior from those for the imaginary potential parameters. This results from the fact that the factors $\partial U/\partial p_i$ are 90° out of phase for these two cases, and therefore they sample different parts of the complex squared wave function.

III. SENSITIVITY ANALYSIS FOR ^{56}Fe

In order to determine the dependence of cross sections on individual optical-model parameters, we carried out sensitivity calculations by computing the derivatives of the total and absorption cross sections with respect to the individual parameters. This can provide guidance for investigating general properties of the optical model as well as exhibiting correlations among the parameters. Our definition of sensitivity is

$$\mathcal{D}(E;p) = \frac{p}{\sigma}\,\frac{\partial\sigma}{\partial p}. \tag{12}$$

This provides an estimate of the fractional change in the cross section $\sigma \equiv \sigma(E;p)$ induced by a given fractional change in the model parameter p. That is, $\Delta\sigma/\sigma \approx \mathcal{D}(E;p)\,\Delta p/p$ for suitably small values of $\Delta p/p$. In the above expressions σ is either $\sigma_{\rm tot}$ or $\sigma_{\rm abs}$.

Using ^{56}Fe as an example, we show results in Fig. 3 for the parameter sensitivities $\mathcal{D}(E;p)$ for nine parameters in the description of the optical potential given by Eqs. (2) and (3). The values of these parameters are taken from the global optical potential of Ref. [4]. Results for the total cross section are shown in the left column of the figure, and those for the absorption are shown on the right. Sensitivities to the potential strengths V_v (real volume), W_v (imaginary volume), and W_s (imaginary surface) are shown in the top row. The second and third rows show results for the corresponding radii (r_v, r_w, r_s) and diffuseness parameters (a_v, a_w, a_s). Although

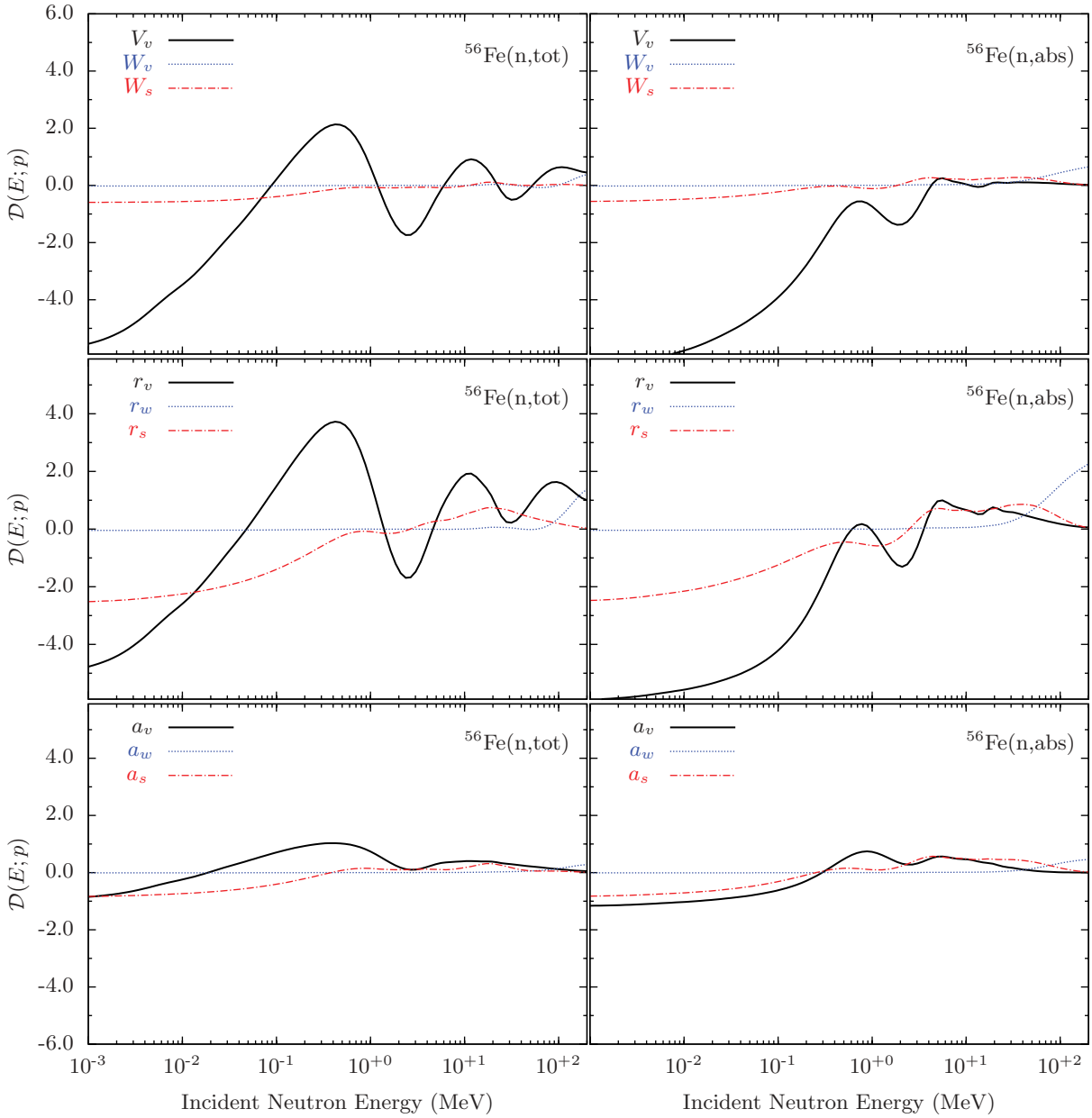

FIG. 3. (Color online) Sensitivity of the $^{56}\mathrm{Fe} + n$ total and absorption cross sections to perturbations of the potential strengths, radii, and diffuseness parameters. $\mathcal{D}$ is the ratio of the fractional change in the cross section to the fractional change in the perturbed parameter; see Eq. (12). For energies at which a curve passes through $\mathcal{D} = 0$, the cross section is completely insensitive to the corresponding parameter.

they were calculated, we do not show the sensitivities to the six spin-orbit parameters. They have negligible effects on the cross sections discussed here, which do not involve spin observables. In this section we make some general remarks about these results, and in the next section show how some of the results are understandable from simple properties of scattering from a complex potential.

We first note that at low energies the sensitivities for the absorption and total cross sections tend toward a common value. This is consistent with the behavior pointed out in the discussion of Eqs. (10) and (11), even though in this case a really close equivalence between the two cross sections is not yet achieved at the lowest energy shown (1 keV). Later we see that a study of the sensitivities as a function of both mass and energy shows that the approximate equality is qualitatively valid up to about 100 keV.

Another feature exhibited by the curves in Fig. 3 is the presence of strong correlations between many of the parameters. This happens when the corresponding curves have approximately the same energy dependence but different magnitude (including the possibility of inversion). A particularly well-known example is the correlation between V_v and r_v, which is seen in the present case. This correlation is often assumed to be of the form $V_v r_v^2 = \text{const}$ for incident energies in the range of several MeV. If this form of the correlation were precisely applicable here, the sensitivity values for r_v

would be twice those for V_v. For the total cross section, we see that this condition is approximately satisfied only in the region ≈5–20 MeV. Outside this region, the correlation is more complicated (note, for example, the upward shift in the r_V sensitivity above 20 MeV). Equation (10) suggests that we should not expect a very simple correlation between V_v and r_v, because the derivatives of the potential in the integrand are of volume form for V_v, but are surface peaked for r_v, and therefore these functions sample the wave function in different ways.

We also see that the sensitivity to the volume imaginary potential is negligible below ≈20 MeV, but becomes the dominant component of the sensitivity to the imaginary potential in the 100–200 MeV region. This simply recognizes the transition from surface to volume form for the imaginary potential with increasing energy, which is found in phenomenological

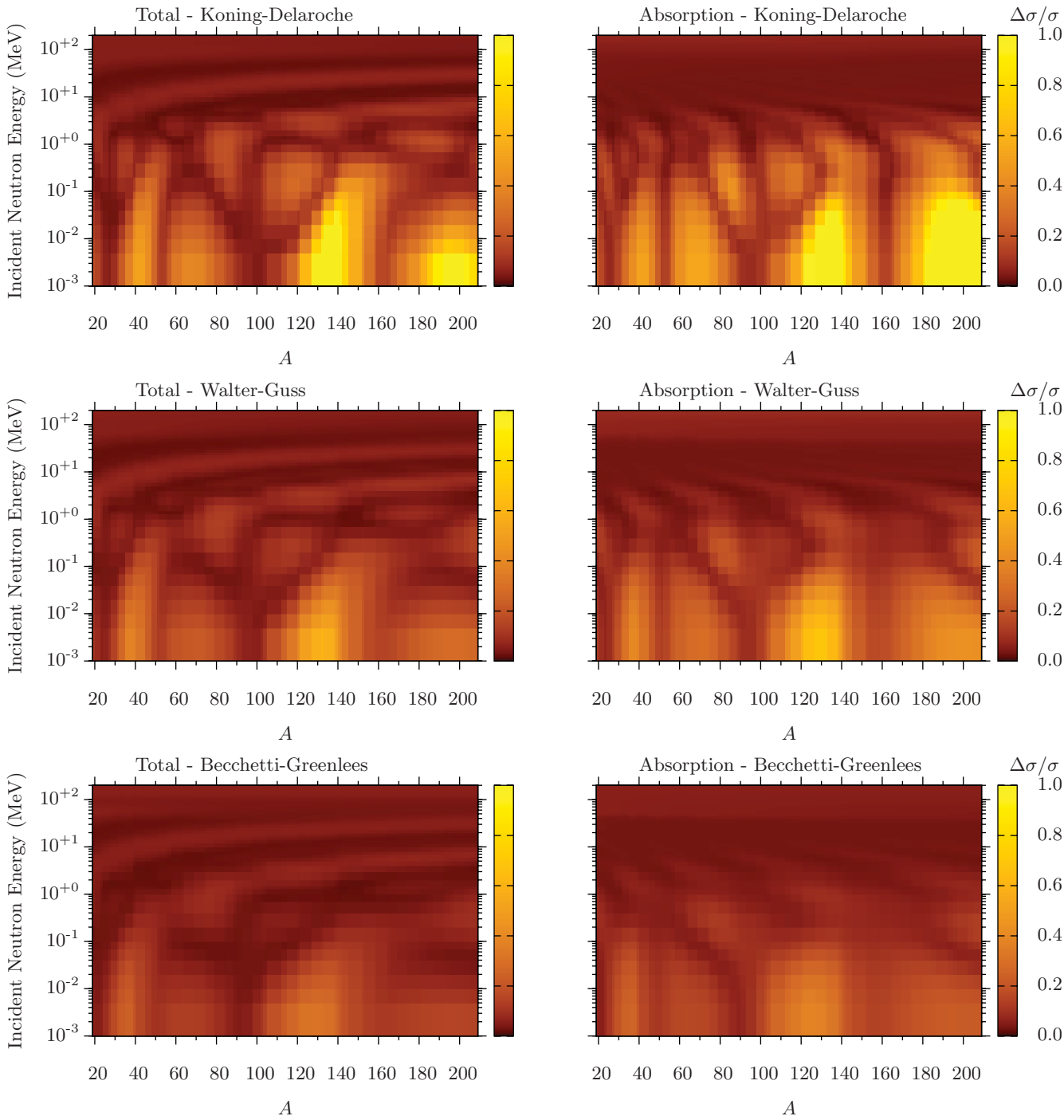

FIG. 4. (Color online) Fractional uncertainties for neutron total cross sections on 75 target nuclei obtained with three different global spherical optical potentials.

optical-model parametrizations as well as in microscopic treatments.

Finally, we note the absence of oscillations above ≈5 MeV in the sensitivity curves for V_v and r_v in the absorption cross section, whereas they are prominent in the total cross section. For sufficiently strong absorption and high enough energies, the cross section is approximately proportional to πR^2, where R is a nuclear radius; thus the cross section is sensitive to the radius parameters, but significantly less so to the strengths. It is also seen that the absorption cross section becomes primarily sensitive to the volume imaginary radius near the uppermost energies (100–200 MeV), which reflects the strengthening of the imaginary potential and weakening of the real potential with increasing energy. The oscillations in the sensitivity of the total cross section to V_v and r_v are discussed in the next section.

IV. ORIGIN OF THE MINIMA

Here we discuss the physical origin of several of the features pointed out in our discussion of ^{56}Fe in the previous section and of the global sensitivity study illustrated in Fig. 1. We also discuss the dependence of the sensitivity minima and maxima on the choice of optical potential.

Figure 4 shows additional information on the sensitivity patterns that will be useful for this discussion. The figure indicates the behavior of the absorption cross section (right column) in addition to the total cross sections (left column) already presented in Fig. 1. It also indicates the sensitivity for two additional global optical potentials (those of Walter and Guss [9] and Becchetti and Greenlees [10]) that preceded the development of the Koning-Delaroche global potential [4]. The quantities actually shown in the figure are a quadratic sum of fractional changes in the cross section resulting from variations of 3% in each of the parameters discussed in the previous section, assuming no correlations among the parameters. We note that the sensitivity minima (dark bands) are very similar for all three optical potentials. These patterns originate predominantly from the properties of the real central potential, since it is much larger than the imaginary central or spin-orbit potentials. We also see that the minima in the total and absorption cross sections are very similar up to at least 100 keV. This is a consequence of the convergence of the total and absorption cross sections in the low-energy limit.

In the following discussion, Section IV A treats the low-energy region ($\lesssim$100 keV), which is dominated by one or a few partial waves. Section IV B deals with a higher-energy region ($\gtrsim$4 MeV), in which many partial waves cooperate to yield a simple result. There does not appear to be a simple interpretation of the sensitivities between these limits. Finally, in Section IV C we make further remarks on the behavior of the sensitivities when different optical potentials are used.

A. Low energies (below approximately 100 keV)

In the region below 100 keV, the features we wish to understand are the vertical bands near $A = 50$ and $A = 160$ and the somewhat more complex, multibranch structures near

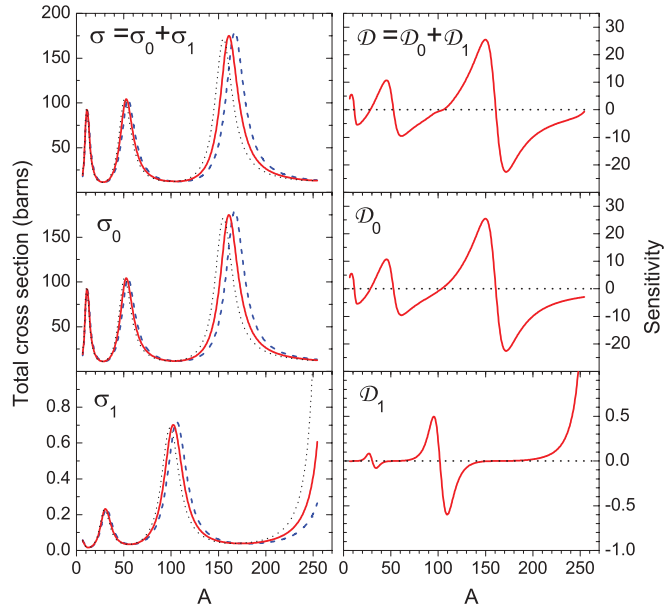

FIG. 5. (Color online) Left column: Total cross section using the optical potential of Ref. [4] for 1-keV neutrons (solid lines); the dotted and dashed lines are calculated with +2% and −2% variations of V_v, respectively. Right column: Sensitivity of total cross section to V_v, as defined by Eqs. (13) and (14). The s- and p-wave parts of these quantities are shown, along with their sum.

$A = 30$ and $A = 100$. These features are simply related to the single-particle resonance structure in the real potential well that gives rise to the well-known strength function peaks as a function of target mass in low-energy neutron scattering (see, for example, Ref. [5]). Figures 5 and 6 show the total cross sections and parameter sensitivities as a function of mass, calculated at 1 and 100 keV, respectively.

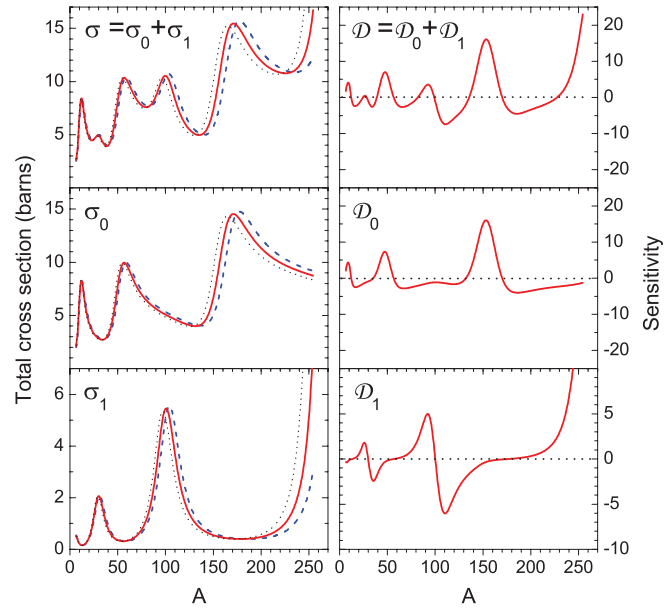

FIG. 6. (Color online) Same as Fig. 5, but for 100 keV instead of 1 keV.

In the left-hand columns of Figs. 5 and 6, the solid line shows the total cross section calculated from the global potential of Ref. [4], as well as its $l = 0$ and $l = 1$ components. The patterns of the maxima and minima in the $l = 0$ and $l = 1$ components are out of phase, in accordance with the alternation of positive- and negative-parity major shells in the single-particle potential. We have also calculated the partial cross sections for $l = 2$ and $l = 3$ and find that they line up well with their $l = 0$ and $l = 1$ parity counterparts, but they are too small to be important for present purposes in the energy range up to ≈100 keV. The dashed and dotted lines show the total cross sections with the strength of the real central potential V_v decreased and increased by 2%, respectively. These variations lead to small shifts of the entire pattern to higher or lower masses. This has the immediate consequence that for both l values there are sensitivity minima at the top of the peaks, as well as between them. This behavior persists as the energy is raised from 1 to 100 keV. However, at the higher energy the s-wave peaks become asymmetric, which causes the between-peaks minimum to shift upward in mass. These s-wave sensitivity minima correspond to those seen in Fig. 4 near $A = 50$ and $A = 160$ and to the rightmost branch of the structures originating from the bottom of the figures near $A = 30$ and $A = 100$.

The remaining structures below approximately 100 keV result from an interplay of the $l = 0$ and $l = 1$ partial cross sections. To see this, it is convenient to define partial-wave sensitivities $\mathcal{D}_l$,

$$\mathcal{D}_l(E; p) = \frac{p}{\sigma}\frac{\partial}{\partial p}\sigma_l(E; p)\,, \tag{13}$$

where σ is the complete cross section and σ_l is the portion of this cross section for orbital angular momentum l. The relation between these partial-wave sensitivities and the sensitivity defined by Eq. (12) is

$$\mathcal{D}(E; p) = \sum_l \mathcal{D}_l(E; p), \tag{14}$$

and the partial cross sections are the total cross sections shown in the left-hand sides of the figures.

The right-hand columns of Figs. 5 and 6 show the full sensitivity $\mathcal{D}$ as well as the partial-wave sensitivities $\mathcal{D}_0$ and $\mathcal{D}_1$ for the total cross sections at 1 and 100 keV. As in the left-hand columns, the varied parameter p is the potential strength V_v. At 1 keV (Fig. 5), the zeros of $\mathcal{D}$ are very close to those of $\mathcal{D}_0$ alone. The effect of the p waves is seen only as a slight change in the slope of $\mathcal{D}$ as it passes through zero near $A = 100$. At 100 keV (Fig. 6), the p-waves play a significant role; note the relative change in the vertical scales between Figs. 5 and 6. In the mass region near $A = 100$, we now see that the structure in the p-wave partial sensitivity, corresponding to the well-known p-wave strength function maximum, leads to two additional zeros in the total sensitivity when added to the s-wave partial sensitivity. These features correspond to the two additional branches in the pattern of sensitivity minima near $A = 100$ in Fig. 4. A similar description applies to the pattern of multiple branching seen near $A = 30$.

The widths of the peaks in Figs. 5 and 6 are determined by the imaginary part of the optical potential. We show the effects

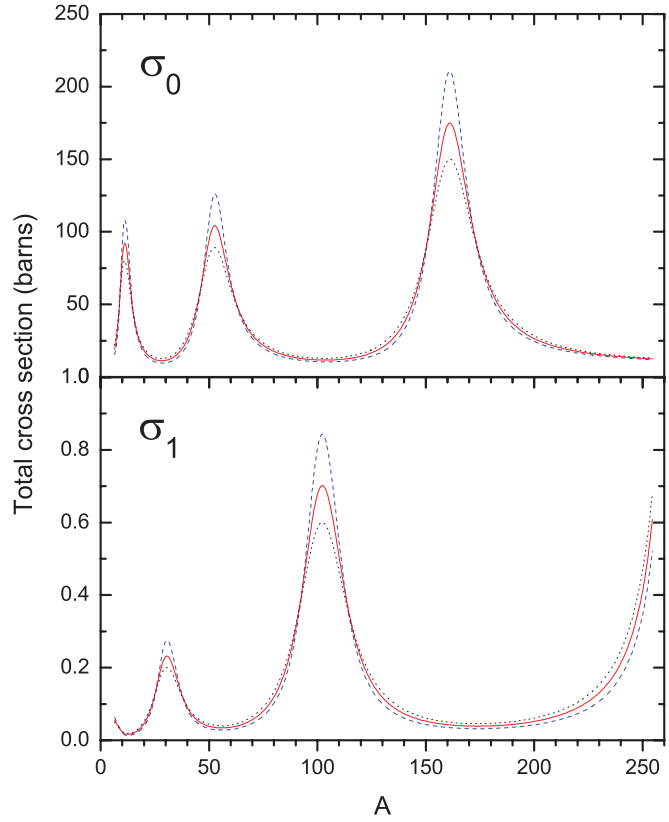

FIG. 7. (Color online) The solid lines are the s- and p-wave parts of the total cross section using the optical potential of Ref. [4] for 1-keV neutrons. The dotted and dashed lines are calculated with +20% and −20% variations of the surface imaginary potential strength W_s, respectively.

of varying the strength of the imaginary surface potential in Fig. 7 for 1-keV total cross sections. As noted earlier, the curves are closely related to the optical-model estimates of the s- and p-wave strength functions. The dashed curve represents a 20% decrease in the strength, while the dotted curve represents a 20% increase. With decreasing damping, the energy of the single-particle states near threshold becomes better defined, resulting in a sharpening of the peak as a function of A. Again there are two sensitivity minima for each peak, but in this case they are located on the sides of the peaks rather than on and between them.

B. High energies (above approximately 4 MeV)

We now turn our attention to the region above approximately 4 MeV, where the sensitivity minima and maxima in the total cross sections in Fig. 5 appear as horizontal stripes. These are easily interpreted via the Ramsauer model, which describes the total cross section by a single phase shift, whose value is determined by the difference in the phase shift between the waves going through the nucleus and those going around it. It accounts for the oscillatory structure seen in the total cross section of ^{56}Fe in Fig. 2 above a few MeV, as well as in all other heavy nuclei. This model has been used [11] to parametrize cross sections in the 6–60 MeV region over a wide mass range

with an accuracy in the neighborhood of 2%, and a study that justifies the assumptions of the model has been carried out [6]. The model is characterized by an effective S matrix and an effective complex phase shift $\delta_{\rm eff}$ as

$$S_{\rm eff}(E) = e^{2i\delta_{\rm eff}(E)} = \alpha(E)\, e^{i\beta(E)}\,, \tag{15}$$

where α and β are real quantities. The total cross section in this model is

$$\sigma_{\rm tot} = 2\pi(R+\lambda)^2(1-\alpha\cos\beta)\,, \tag{16}$$

where R is the nuclear radius. The parameter α is less than 1, which accounts for absorption as well as a correction due to the averaging of the many phase shifts in the actual problem to yield the single phase shift of the model. Fits to 21 nuclei [11] from $A = 40$ to 238 have parametrized it as energy independent and with a slow mass dependence as $\alpha = 0.18$–$0.013A^{1/3}$. In [11] the phase angle β was parametrized as

$$\frac{\beta}{A^{1/3}} = c\,[(\sqrt{a+bE}-\sqrt{E}) + k'(\sqrt{a+bE}-\sqrt{E})^2], \tag{17}$$

where c is another radius parameter, a is closely related to the strength of the real potential well, and b is a parameter whose deviation from unity simulates the energy dependence of the potential strength. The first term is proportional to the difference in wave numbers inside and outside the nucleus; the second term is a small empirical correction that is quadratic in this difference. Values for all of the parameters may be found in Table III of Ref. [11].

We exhibit the sensitivity properties of the Ramsauer model for the case of ^{56}Fe by studying the variation of the total cross section with respect to small changes in a and α, because these are the parameters governing the effects of the real and absorptive parts of an optical potential, respectively. The Ramsauer-model total cross section, divided by the black nucleus cross section, is shown in the top panel of Fig. 8. The bottom panel shows the sensitivities $\mathcal{D}(\alpha) = (\alpha/\sigma)(\partial\sigma/\partial\alpha)$ (solid curve) and $\mathcal{D}(a) = (a/\sigma)(\partial\sigma/\partial a)$ (dashed curve). Parameter values from Ref. [11] were used; in particular $\alpha = 0.13$ and $a = 35.0$ MeV. Because α simply controls the amplitude of the Ramsauer oscillation with energy, its sensitivity pattern should follow the shape of the original oscillation. On the other hand, a small change in a shifts the phase of the oscillation, and thus its sensitivity pattern should be out of phase with the original oscillations. Both of these effects are seen in the figure.

The sensitivity bands apparent in the total cross sections of Fig. 4 above a few MeV, which are adequately described by the Ramsauer oscillations, are absent in the absorption cross sections shown in the figure. This follows from the fact that the nucleus is rather strongly absorbing in all partial waves that can penetrate the nucleus, leading to an approximately constant

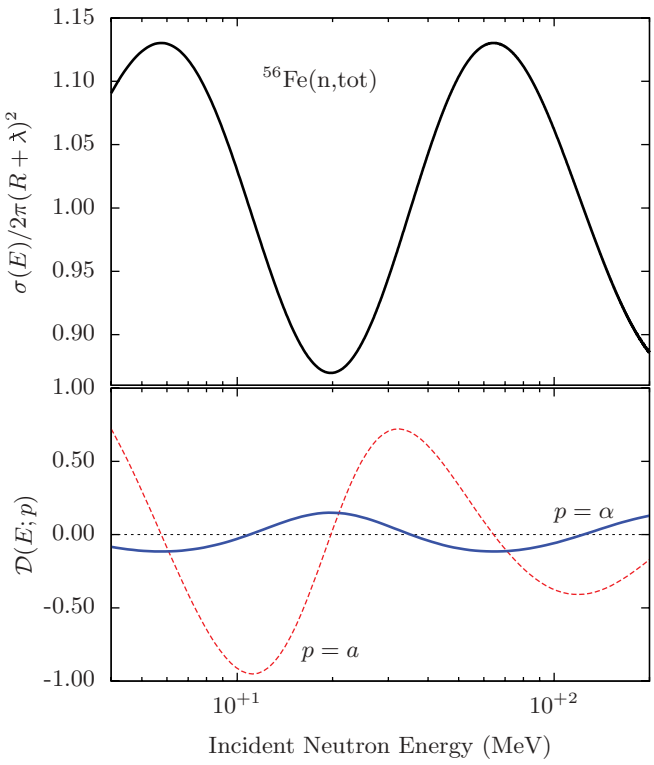

FIG. 8. (Color online) Neutron total cross sections $\sigma_{\rm tot}$ of ^{56}Fe defined in Eq.(16), divided by the black-nucleus value. Bottom: Total cross-section sensitivities obtained by perturbing the parameters α(solid line) and a (dashed line) in Eqs. (16) and (17). The radius R is $1.415A^{1/3}$fm.

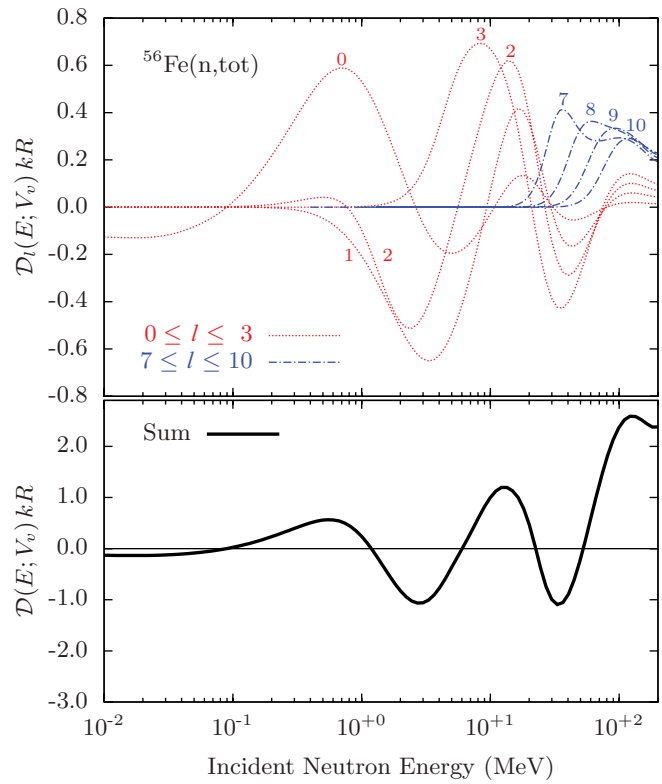

FIG. 9. (Color online) Sensitivity of the ^{56}Fe + n total cross section to a perturbation of the real central potential strength, V_v. The upper panel shows the partial-wave sensitivities for two groups of l values, and the bottom panel shows the total sensitivity. For clarity, the curves are multiplied by kR, where k is the wave number and R is $1.415A^{1/3}$ fm.

cross section in the neighborhood of πR^2 and a consequent lack of pronounced structure when optical parameters are varied.

Figure 9 shows the contributions of the different partial waves to the total sensitivity for the case of ^{56}Fe, calculated from the optical model of Ref. [4] . The upper panel shows the partial sensitivity for two groups of partial waves, $l = 0 - 3$ and $l = 7 - 10$, and the lower panel shows the sum of all partial waves. Since ^{56}Fe is near a peak in the s-wave strength function and a minimum in the p-wave, a single partial wave ($l = 0$) dominates the sensitivity up to several hundred keV, in a manner consistent with the discussions of Figs. 5 and 6. Above several MeV, we see the contributions from the various partial waves developing a simple pattern that leads to the Ramsauer description. In between these limits, the total sensitivity is determined by a small group of partial waves whose behavior is not amenable to a simple description.

C. Sensitivity to choice of optical potential

Even though the locations of the sensitivity minima are very similar for the three potentials shown in Fig. 4, there are remaining differences in the magnitudes of the sensitivity away from the minima. This is shown more clearly in Fig. 10 which shows the sensitivity of the total cross sections to perturbation of the parameters of four global optical potentials for ^{56}Fe. These potentials and their stated or estimated range of applicability [13] are those of Koning and Delaroche [4] (1 keV to 200 MeV), Becchetti and Greenlees [10] (10–50 MeV), Wilmore and Hodgson [12] (10 keV to 25 MeV), and Walter and Guss [9] (10–80 MeV). As was the case for Fig. 4, the curves represent the uncertainty $\Delta\sigma/\sigma$ resulting from the addition in quadrature of the variations in cross section resulting from 3% variations in each of the nine parameters; however, the variations with strength and radius of the real central potential are dominant. We see that the older optical potentials behave rather similarly to the Koning-Delaroche within their ranges of applicability as stated above. The Becchetti-Greenlees potential is known to have a surface imaginary potential that is much too large to correctly describe neutron data below 10 MeV, which is likely to account for the particularly small values of the uncertainties between the minima. However, the maxima and minima in the total cross-section uncertainties occur at nearly the same energies for all of the potentials. This is a consequence of the fact that the shape and strength of the dominant real central potential are well determined, even for rather old optical potentials that were fit to a limited set of data.

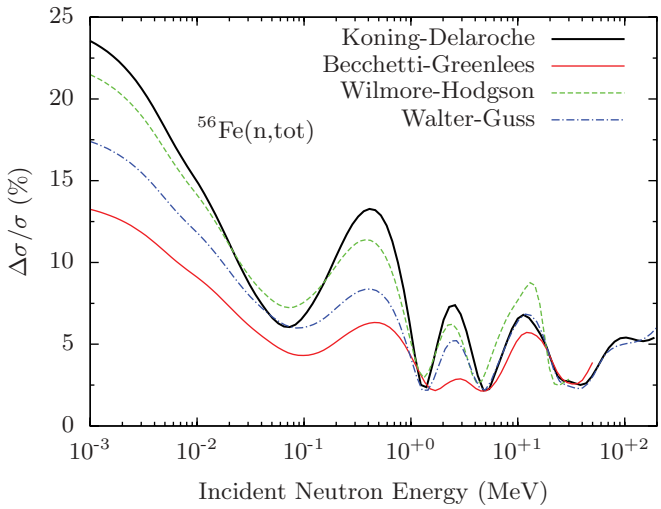

FIG. 10. (Color online) Fractional total cross section uncertainties of ^{56}Fe + n obtained by perturbing the optical model parameters for different global potentials [4,9,10,12]

V. SUMMARY AND CONCLUSIONS

We have investigated the physical origin of the minima that were obtained in a study of the sensitivity of the neutron total and absorption cross sections to small changes in the optical model parameters used to calculate them. These minima appear for all nuclei and are a general property of optical potentials rather than of a specific parametrization. To understand these features we have studied the predictions of a particular global optical potential [4] over a wide mass and energy range. We have also taken a more detailed look at one specific nucleus, ^{56}Fe.

In the limit of very low energies, the total and absorption cross sections coincide. We find that the sensitivity properties of the total and absorption cross sections are qualitatively very similar up to about 100 keV, after which they diverge.

We have found simple physical interpretations for the behavior of the sensitivity minima and maxima in two energy ranges. In the first, below approximately 100 keV, the sensitivity patterns are determined largely by the properties of the s- and p-wave states in the real potential well. These also give rise to the s- and p-wave strength functions derived from low-energy neutron resonance properties. Above approximately 4 MeV the structure in the total cross-section sensitivities (and lack of structure for the corresponding absorption cross sections) is consistent with the Ramsauer model, which is a simple single-phase-shift model that describes the observed oscillations in total cross sections with energy. Between these low- and high-energy limits, the behavior of the sensitivities results from the interplay of a few partial waves and does not appear to have a simple interpretation.

We have compared the sensitivity properties obtained from the Koning-Delaroche potential [4] with those from several older global potentials that were designed for limited energy ranges. We find that their sensitivity minima are close to those from the more recent potential, but that they vary in the degree of sensitivity in the regions of mass and energy away from the minima.

We anticipate that the structure of the sensitivities identified in this study can be useful in future studies of optical-model parametrization and applicability. The regions near the sensitivity maxima are the most useful for determining the model parameters from experimental input and data analysis. On the other hand, analyzing data near the sensitivity minima is potentially important for revealing phenomena that are not within the scope of the optical model, such as the effects of doorway states.

ACKNOWLEDGMENTS

The present work was supported by the DOE-NNSA within the Nuclear Criticality Safety Program and this support is gratefully acknowledged. The National Nuclear Data Center is sponsored by the Office of Nuclear Physics, Office of Science of the US Department of Energy under Contract DE-AC02-98CH10886 with Brookhaven Science Associates, LLC. Part of this work was performed under the auspices of the US Department of Energy by the Lawrence Livermore National Laboratory under Contract DE-AC52-07NA27344.

[1] W. Hauser and H. Feshbach, Phys. Rev. **87**, 366 (1952).
[2] R. Capote *et al.*, Nucl. Data Sheets **110**, 3107 (2009).
[3] M. T. Pigni, M. Herman, and P. Obložinský, Nucl. Sci. Eng. **162**, 25 (2009).
[4] A. J. Koning and J.-P. Delaroche, Nucl. Phys. A **713**, 231 (2003).
[5] S. F. Mughabghab, *Atlas of Neutron Resonances*, 5th ed. (Elsevier, Amsterdam, 2006).
[6] S. M. Grimes, J. D. Anderson, R. W. Bauer, and V. A. Madsen, Nucl. Sci. Eng. **130**, 340 (1998).
[7] M. B. Chadwick *et al.*, Nucl. Data Sheets **107**, 2931 (2006).
[8] L. S. Rodberg and R. M. Thaler, *Introduction to the Quantum Theory of Scattering* (Academic Press, New York, 1967).
[9] R. L. Walter and P. P. Guss, Radiat. Eff. **95**, 73 (1985).
[10] F. D. Becchetti Jr., and G. W. Greenlees, Phys. Rev. **182**, 1190 (1969).
[11] R. W. Bauer, J. D. Anderson, S. M. Grimes, D. A. Knapp, and V. A. Madsen, Nucl. Sci. Eng. **130**, 348 (1998).
[12] D. Wilmore and P. E. Hodgson, Nucl. Phys. **55**, 673 (1964).
[13] *Handbook for Calculations of Nuclear Reaction Data, RIPL-2*, Technical Report IAEA-TECDOC-1506 (IAEA, Vienna, 2006).